University of Pretoria etd – Agyei N M 2004

CHAPTER 7

RESULTS AND DISCUSSION: PHOSPHATE REMOVAL BY OPC

7.1. Particle dimensions and chemical composition

Figure 7.1 shows the distribution function for the OPC, obtained by Fraunhofer diffraction particle analysis as described in Experimental Section 4.3.1.

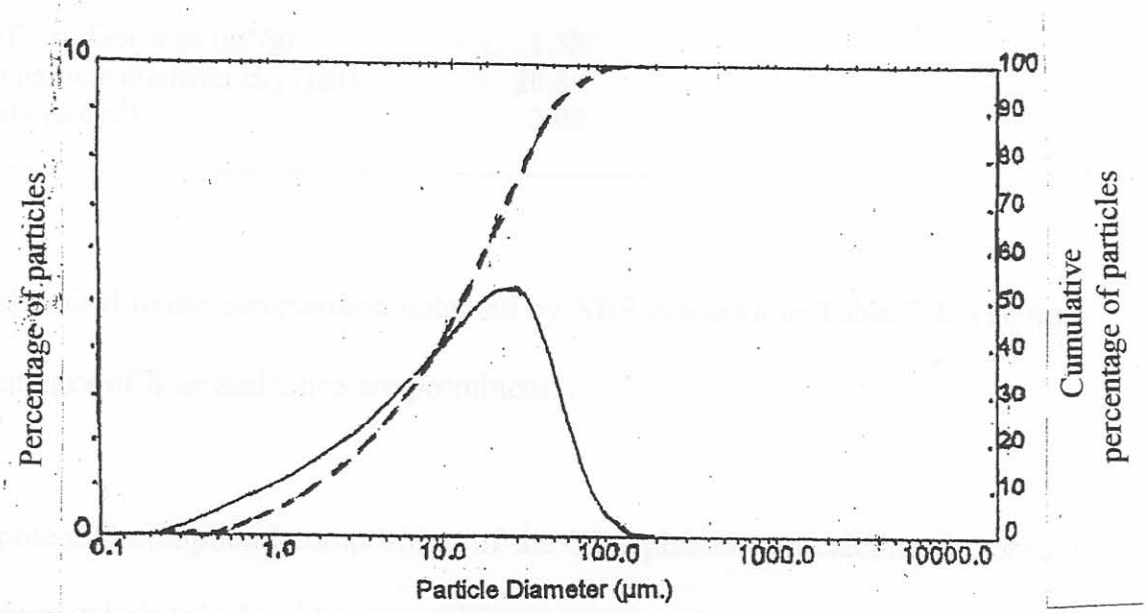

Figure 7.1. Particle size distribution for the OPC sample.

The solid line represents the percentage of particles having a given diameter, the particle size distribution being a logarithmic function of the individual particle sizes (see equation (3.1)). Its shape approximates a log-normal curve, albeit slightly skewed towards lower particle sizes. The broken line is a cumulative curve that represents the percentage of particles whose diameters are less than a

University of Pretoria etd – Agyei N M 2004

given diameter. About 65 % of the particles were found to have diameters in the 5-50 μm size range.

Some important physical properties are summarised in Table 7.1.

Table 7.1. Physical properties of OPC.

Characteristic	Value
Specific surface area (m^2/g)	1.38
Mean particle diameter $d_{4,3}$ (μm)	20.8
Density (g/cm^3)	3.02

The chemical oxide composition obtained by XRF is shown in Table 7.2. The high percentages of lime and silica are prominent.

The potential compound composition of the OPC phases was calculated from the experimental chemical oxide composition data using the Bogue (1955) equations. The values obtained for the major phases, namely, alite (C_3S), belite (C_2S), aluminate (C_3A) and ferrite (C_4AF) are given in Table 7.3.

University of Pretoria etd – Agyei N M 2004

Table 7.2. Chemical oxide composition of OPC.

Component	Mass %
SiO_2	22.5
Al_2O_3	4.5
Fe_2O_3	1.4
Mn_2O_3	0.9
TiO_2	0.2
CaO	63.2
MgO	3.6
P_2O_5	0.2
SO_3	2.4
Cl	<0.1
K_2O	0.8
Na_2O	0.1
LOI @ 1000°C	1.0
Total	100.8

Table 7.3. Potential compound composition of OPC.

Phase	Mass %
C_3S	54.0
C_2S	23.8
C_3A	9.6
C_4AF	4.3

7.2. Kinetics

Figure 7.2 illustrates the percentage PO_4^{3-} removed with time, measured as described in Experimental Section 4.3.4. It can be seen that the uptake of PO_4^{3-}

University of Pretoria etd – Agyei N M 2004

virtually ceased after a contact time of about 3 hrs, indicating the establishment of dynamic equilibrium. The fractional attainment of equilibrium as a function of time, assuming a first order reversible kinetics model, is given by equation (1.12) as explained in Section 1.3.

A plot according to equation (1.12) is shown in Figure 7.3.

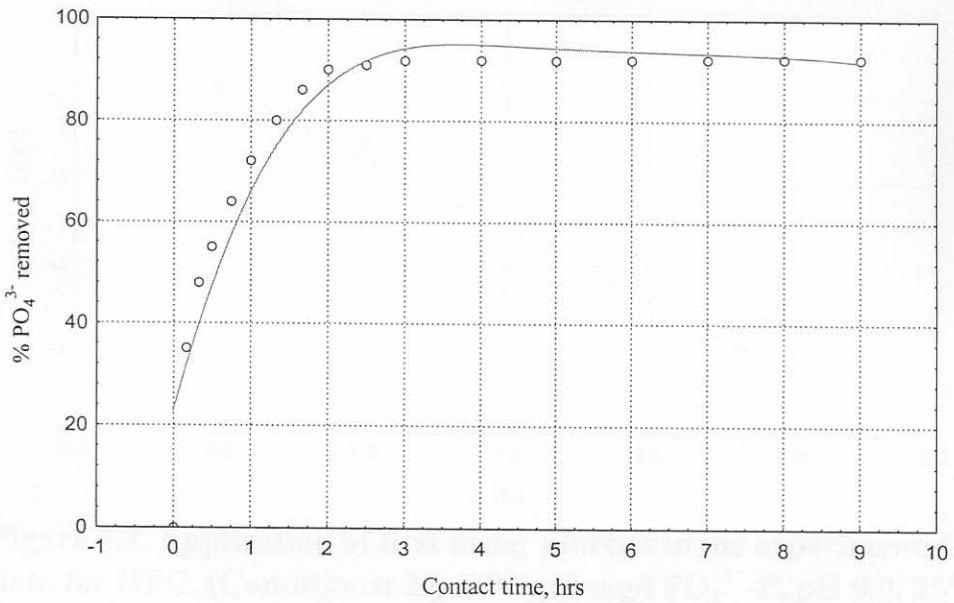

Figure 7.2. Kinetics of PO_4^{3-} removal by OPC.
(Conditions: 2 g OPC, 80 mg/l PO_4^{3-}-P, pH 9.0, 25°C)

The reasonably good straight-line fit observed (R^2= 0.994) indicates that the sorption reaction may be approximated by first order reversible kinetics; the calculated rate constant is given in Table 7.4.

University of Pretoria etd – Agyei N M 2004

Table 7.4. Values of first order reaction rate constant and intra-particle diffusion constant for removal by OPC.

Parameter	Value
k' (per hour)	1.682
D (cm^2/s)	8.72×10^{-11}

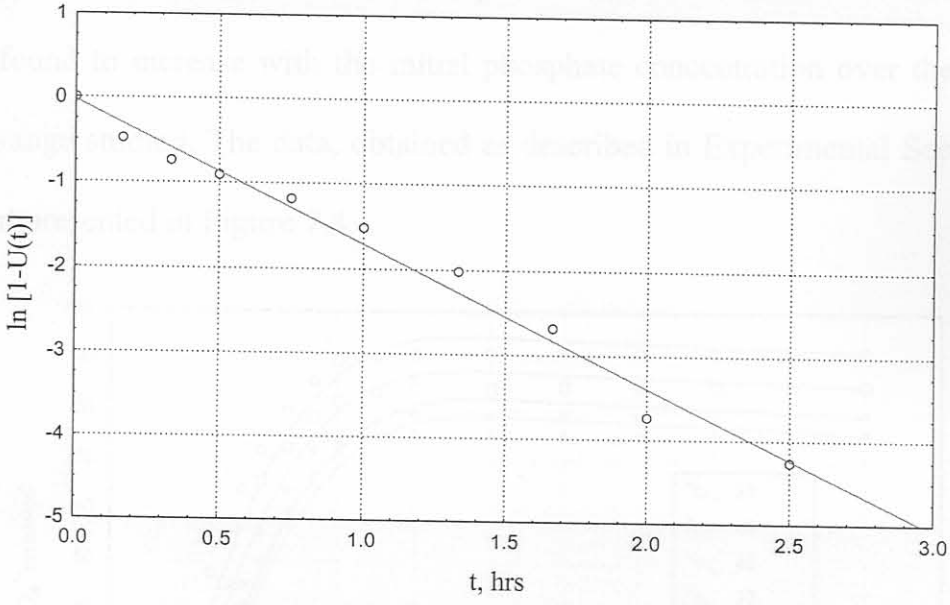

Figure 7.3. Application of first order kinetics to the experimental adsorption data for OPC. (Conditions: 2 g OPC, 80 mg/l PO_4^{3-}-P, pH 9.0, 25°C)

Over the range of sorbent-solution agitation rates studied (100-140 cycles per minute horizontally) it was observed that the sorption rate was not affected by the rate of mixing. This suggests that diffusion in the pores of sorbent particles rather than diffusion through the film at the sorbent particle-aqueous solution interface is rate limiting, which would provide evidence that intra-particle diffusion is the controlling resistance rather than external diffusion.

University of Pretoria etd – Agyei N M 2004

The value of the intra-particle diffusion constant D calculated using equation (1.13) is given in Table 7.3.

7.3. Effect of concentration

The rate and separation efficiency of PO_4^{3-} from aqueous solution by OPC was found to increase with the initial phosphate concentration over the concentration range studied. The data, obtained as described in Experimental Section 4.3.5.1, is represented in Figure 7.4.

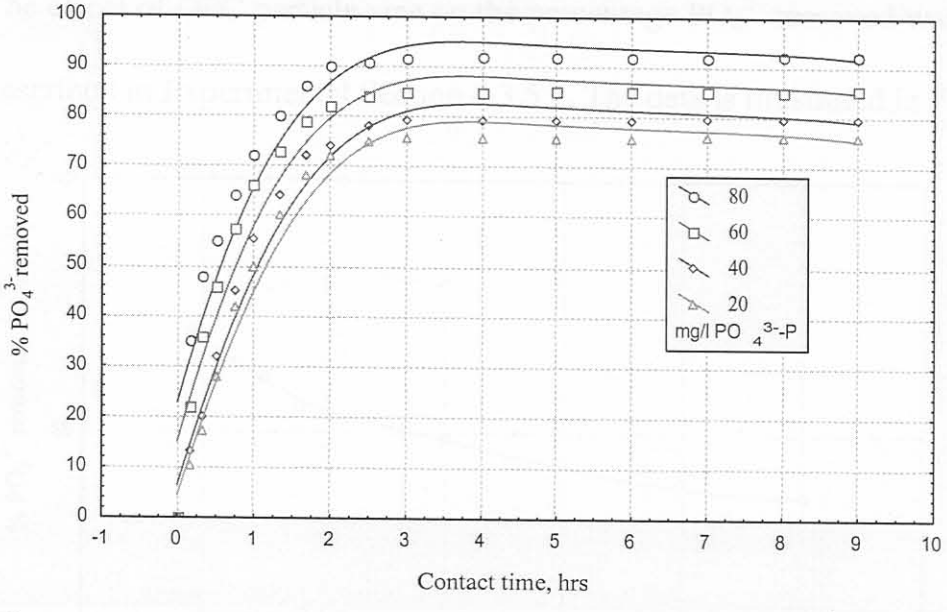

Figure 7.4. Effect of concentration on the kinetics of PO_4^{3-} removal by OPC. (Conditions: 2 g OPC, pH 9.0, 25°C)

The observed increase in the percentage PO_4^{3-} removed with increasing solute concentration (for the same amount of sorbent) is hardly surprising if the system

University of Pretoria etd – Agyei N M 2004

under study is non-ideal. As mentioned in Sections 1.2.1 and 1.2.2, for non-ideal systems the mass of solute adsorbed per mass of sorbent keeps increasing as the concentration of the solute increases. This has been ascribed to surface heterogeneity in such systems. Interestingly, the initial phosphate concentration does not appear to influence the time it takes (ca 3 hrs) for PO_4^{3-} removal to reach equilibrium.

7.4. Effect of particle size

The effect of OPC particle size on the percentage PO_4^{3-} removed was measured as described in Experimental Section 4.3.5.2. The data is illustrated in Figure 7.5.

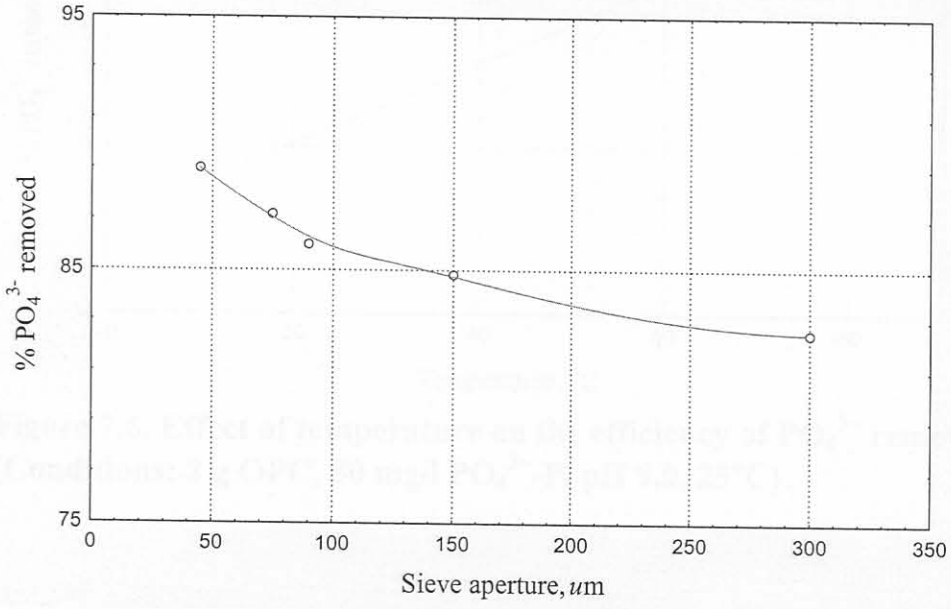

Figure 7.5. Effect of particle size on the efficiency of PO_4^{3-} removal by OPC. (Conditions: 2 g OPC, 80 mg/l PO_4^{3-}-P, pH 9.0, 25°C)

University of Pretoria etd – Agyei N M 2004

Although there was some increase in the percentage PO_4^{3-} removed as the particle size decreased, this increase does not appear to be proportional to the increased surface area.

7.5. Effect of temperature

The effect of temperature on the efficiency of PO_4^{3-} removal was measured as described in Experimental Section 4.3.5.3, and the data is illustrated in Figure 7.6.

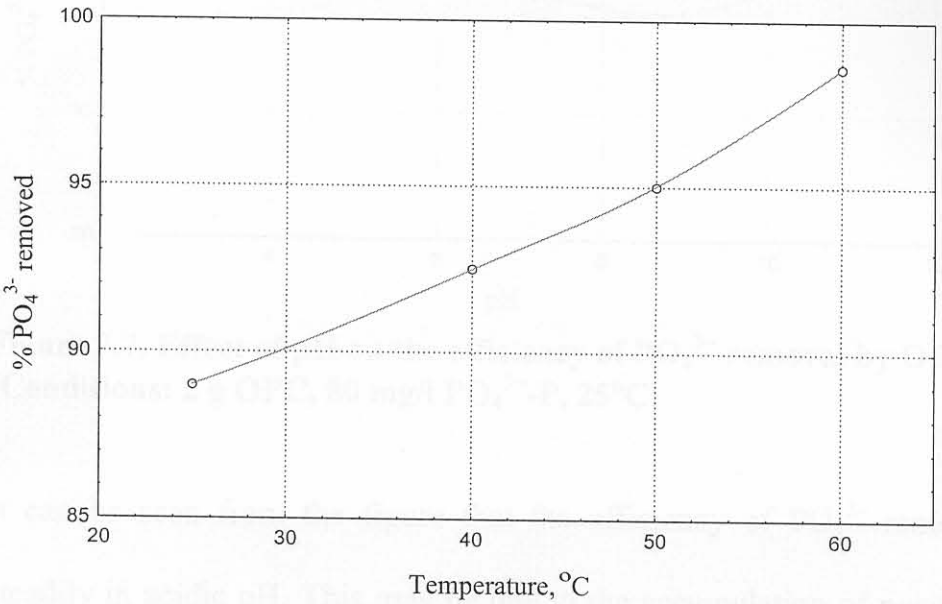

Figure 7.6. Effect of temperature on the efficiency of PO_4^{3-} removal by OPC. (Conditions: 2 g OPC, 80 mg/l PO_4^{3-}-P, pH 9.0, 25°C)

The percent PO_4^{3-} removed was observed to increase with temperature, which is to be expected as the rate of diffusion increases with increasing temperature.

University of Pretoria etd – Agyei N M 2004

7.6. Effect of pH

The variation of the percentage PO_4^{3-} removed with the initial pH of the aqueous solution was measured as described in Experimental Section 4.3.5.4. The data obtained for OPC is shown in Figure 7.7.

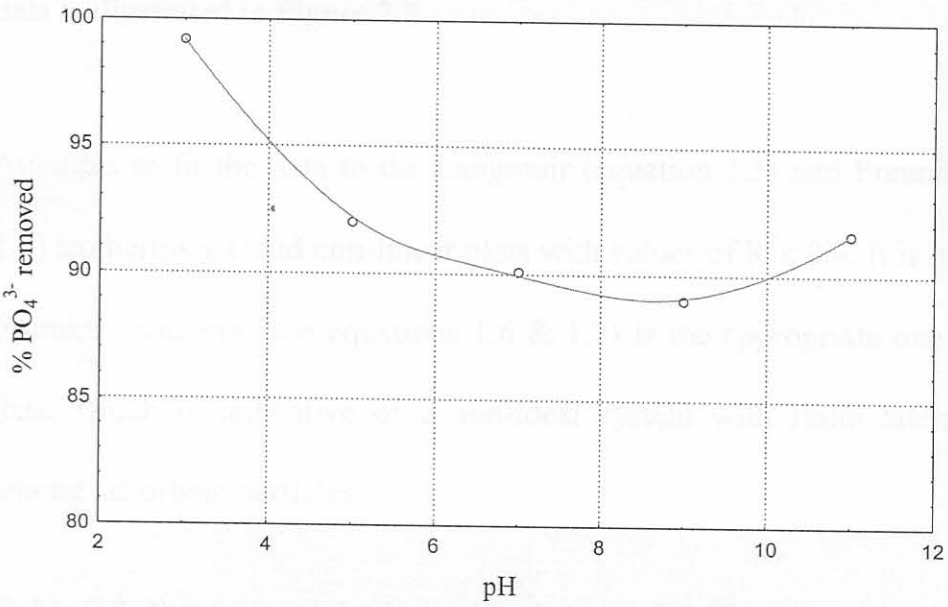

Figure 7.7. Effect of pH on the efficiency of PO_4^{3-} removal by OPC. (Conditions: 2 g OPC, 80 mg/l PO_4^{3-}-P, 25°C)

It can be seen from the figure that the efficiency of PO_4^{3-} removal increases steadily in acidic pH. This may be due to the accumulation of positive charge on the adsorbent surface that increases its affinity for the negatively charged phosphate ions. The observed slight increase in the efficiency of PO_4^{3-} removal beyond pH 9 could be due to the creation of favourable conditions for calcium phosphate precipitation at high pH, thus enhancing the removal of PO_4^{3-} by some dissolved calcium formed by hydration of OPC.

University of Pretoria etd – Agyei N M 2004

7.7. Adsorption isotherms

Adsorption data for modelling adsorption isotherms was obtained as described in Experimental Section 4.3.6. Table 7.5 shows the experimentally obtained adsorption data for fly ash, and the application of the Frumkin equation (1.7) to the data is illustrated in Figure 7.8.

Attempts to fit the data to the Langmuir (equation 1.3) and Freundlich (equation 1.4) isotherms yielded non-linear plots with values of $R^2 < 0.4$. It is evident that the Frumkin isotherm (see equations 1.6 & 1.7) is the appropriate one for fitting the data, which is indicative of a non-ideal system with finite lateral interactions among adsorbate particles.

Table 7.5. Experimental adsorption data for PO_4^{3-} removal by OPC.

mass of fly ash (g)	mg/l P[a] after adsorption	mg P[a] adsorbed
0.5	34.4	13.1
2	32.2	13.6
3	31.1	13.8
3.5	28.2	14.4
4	15.6	16.9
5	0.4	19.9

[a] PO_4^{3-} (as P)

The Frumkin constants were calculated and are shown in Table 7.6.

University of Pretoria etd – Agyei N M 2004

Table 7.6. Isotherm linear correlation coefficients and Frumkin constants for PO_4^{3-} adsorption by OPC.

Isotherm	R^2	α	β
Frumkin	0.995	4.976	0.004
Langmuir	0.269		
Freundlich	0.139		

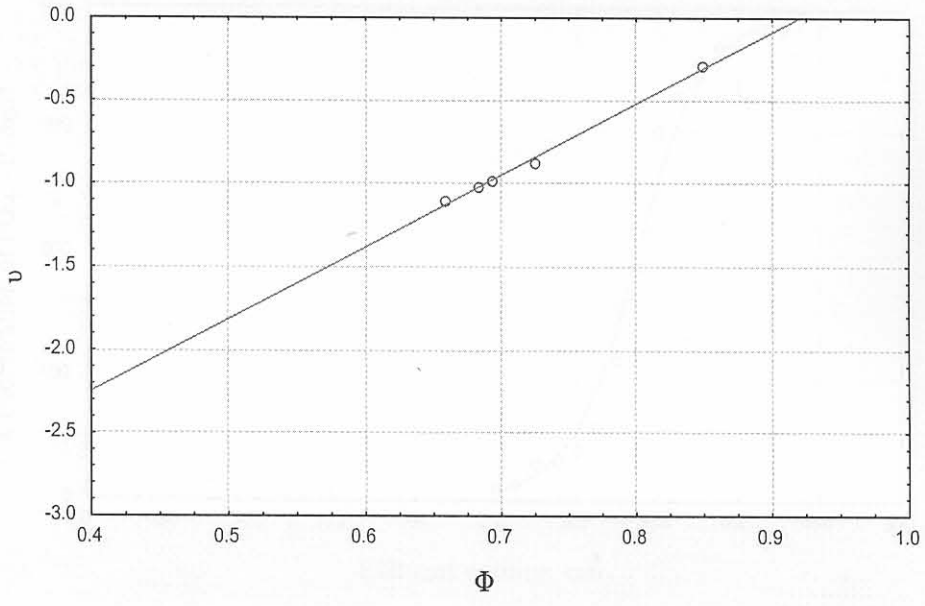

Figure 7.8. Application of the Frumkin equation to the experimental adsorption data (given in Table 7.4) for OPC.

7.8. Breakthrough curves

Data for constructing breakthrough curves was obtained as described in Experimental Section 4.3.7. The data obtained from the breakthrough experiments (see equations 1.15 and 1.16) for OPC are shown in Table 7.7, and a representative breakthrough curve is illustrated in Figure 7.9.

University of Pretoria etd – Agyei N M 2004

Table 7.7. Breakthrough data for OPC.

t_E[a] (min)	V_T (cm^3)	V_Z (cm^3)	h_Z (cm)	C_T (mg PO_4^{3-}-P/g)
10.8	412	1142	0.833	83

[a]Breakthrough time

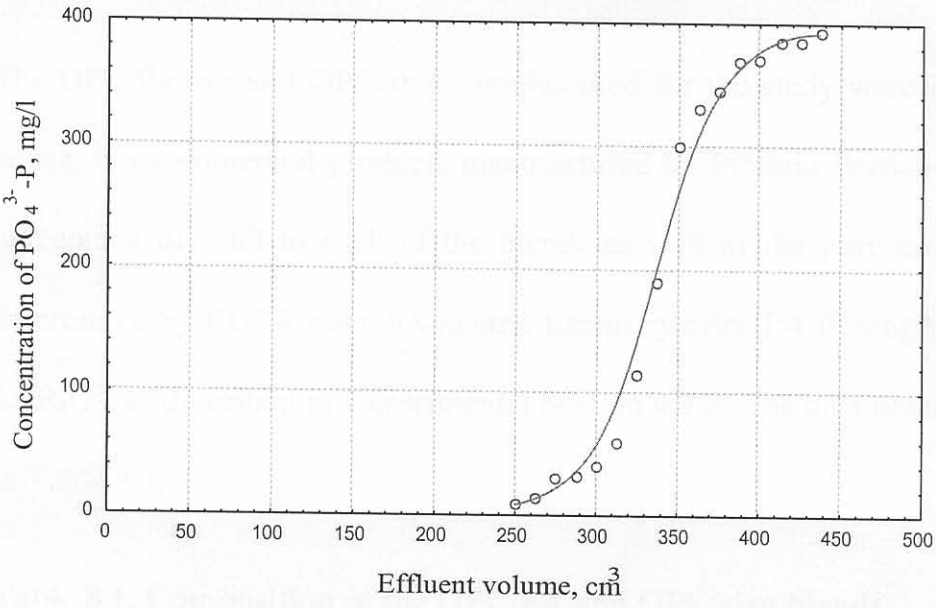

Figure 7.9. Breakthrough curve for PO_4^{3-} removal by OPC.

The curves obtained were good approximations for characteristic symmetrical breakthrough *S* curves. Average values obtained for the breakthrough time t_E, the effluent volume required for bed exhaustion V_T, V_Z (V_T minus the effluent volume required for breakthrough), the height of the mass transfer zone h_Z, and the adsorption capacity C_T are given in Table 7.7.

An average C_T value of 83 mg PO_4^{3-}-P/g was obtained for the OPC.